

Asymmetry in Directional Spreading Function of Random Waves due to Refraction

Changhoon Lee¹; Jae-Sang Jung²; and Merrick C. Haller³

Abstract: In this study, a more general directional spreading function is developed that allows for asymmetric directional distributions. For multidirectional random waves that approach the shore obliquely over a planar slope, we demonstrate that directional asymmetry is generated due to wave refraction. The asymmetry created by refraction increases with the offshore peak wave direction. The present spreading function is compared to a preexisting symmetric spreading function and is shown to better capture changes in the directional distribution that occur in a refracting, random wave field. Finally, the new asymmetric spreading function is compared to a long time series of wave directional spectra measured at a nearshore field site. The results demonstrate that refraction-induced asymmetry is common in the nearshore and the asymmetric spreading function gives an improved analytic representation of the overall directional distribution as compared to the symmetric function.

DOI: 10.1061/(ASCE)WW.1943-5460.0000006

CE Database subject headings: Asymmetry; Wave refraction; Random waves.

Author keywords: Directional asymmetry; Refraction; Numerical experiment; Multidirectional random waves.

Introduction

Water waves generated by the wind are multidirectional random waves. The wave energy increases with the wind speed, duration, and fetch. In regions of active generation, the peak wave direction is aligned with the wind direction and the initial directional spreading is generally symmetric about the peak direction. The wave energy distribution in frequency and direction is given by the directional spectrum $S(f, \theta)$, which can be represented as the product of the frequency spectrum $S(f)$ and the directional spreading function $G(f, \theta)$. Analytic models for the shape of the frequency spectrum are many and include the Pierson-Moskowitz spectrum (Pierson and Moskowitz 1964), the Bretschneider-Mitsuyasu spectrum (Bretschneider 1968; Mitsuyasu, 1970), the Joint North Sea Wave Project (JONSWAP) spectrum (Hasselmann et al. 1973), and the TEXEL storm, MARSEN, ARSLOE (TMA) spectrum (Bouws et al. 1985), etc. The TMA spectrum is unique in that it was developed as modification to the JONSWAP spectrum to include the effect of shoaling on the frequency distribution. It does not, however, include the effect of refraction. The other analytic models were developed strictly for deep water conditions. Analytic directional spreading functions take the form

$\cos^2(\theta - \theta_p)$ (Pierson et al. 1952), $\cos^{2s}[(\theta - \theta_p)/2]$ (Longuet-Higgins et al. 1961), and $\cos^{2s}(\theta - \theta_p)$ (Borgman 1969), where s = directional spreading parameter; and θ_p = peak wave direction and is taken to be the same for all frequencies in the distribution. Mitsuyasu et al. (1975) suggested the value of s based on measured field data. These directional spreading functions all impose directional symmetry about the peak wave direction.

For many engineering applications, measured directional spectra are not available and designers have only bulk estimates of wave height, period, and direction. For these applications analytic models for wave directional spectra can be used to generate representative wave conditions. It is important that these analytic models accurately represent the wave directional spreading in coastal areas, since damage predictions for coastal structures are sensitive to the directional characteristics of the design wave field, as shown by Suh et al. (2002) and Vugts (2005). Van Dongeren et al. (2003) also demonstrate the importance of wave directional spreading in the generation of long waves in the surf zone. It should be noted that the imposition of directional symmetry will degrade their accuracy in areas where wave refraction is important. Goda and Suzuki (1975) showed that the directional spreading function becomes narrower as waves propagate over a planar slope. Their directional spreading function assumes directional symmetry. However, multidirectional random wave spectra will become more directionally asymmetric in shallower water due to the difference in refraction of directionally symmetric components.

In this study, we develop a directional spreading function that considers directional asymmetry as well as symmetry. The purpose of the new spreading function is to serve as an initialization point for modeling or engineering design work. In "Development of Directional Spreading Function Which Considers Directional Asymmetry," the directional spreading function is developed. In "Refraction of Multidirectional Random Waves over a Planar Slope," asymmetry of directional distribution is found and comparisons are made between the predictions by the present spreading function and the previous function. In "Comparison of

¹Associate Professor, Dept. of Civil and Environmental Engineering, Sejong Univ., 98 Kunja-dong, Kwangjin-gu, Seoul 143-747, South Korea (corresponding author). E-mail: clee@sejong.ac.kr

²Assistant Manager, Civil Engineering Team, Hyundai Development Company, 160 Samsung-dong, Gangnam-gu, Seoul 135-881, South Korea. E-mail: fingon@hyundai-dvp.com

³Associate Professor, School of Civil and Construction Engineering, Oregon State Univ., Corvallis, OR 97331. E-mail: hallerm@enr.orst.edu

Note. This manuscript was submitted on August 16, 2008; approved on January 16, 2009; published online on February 24, 2009. Discussion period open until June 1, 2010; separate discussions must be submitted for individual papers. This paper is part of the *Journal of Waterway, Port, Coastal, and Ocean Engineering*, Vol. 136, No. 1, January 1, 2010. ©ASCE, ISSN 0733-950X/2010/1-1-9/\$25.00.

Suggested Directional Spectra to Field Data,” it is found that directional asymmetry is common in refracted near-shore wave spectra and that including asymmetry in the present distribution function leads to a better fitting of the measured data. In “Conclusion,” concluding remarks are made with a discussion for further study.

Development of Directional Spreading Function Which Considers Directional Asymmetry

Multidirectional random waves can be expressed by the directional spectrum $S(f, \theta)$ given by

$$S(f, \theta) = S(f)G(f, \theta) \quad (1)$$

where $S(f)$ =frequency spectrum and $G(f, \theta)$ =directional spreading function, which has been found to vary with frequency. A commonly used directional spreading function was developed by Longuet-Higgins et al. (1961) as

$$G(f, \theta) = G_0 \cos^{2s} \left(\frac{\theta - \theta_p}{2} \right) \quad (2)$$

where

$$G_0 = \left[\int_{\theta_{\min}}^{\theta_{\max}} \cos^{2s} \left(\frac{\theta - \theta_p}{2} \right) \right]^{-1} \quad (3)$$

which is symmetric about the peak direction θ_p . By fitting to deep water wave data, Mitsuyasu et al. (1975) suggested the spreading parameter s as

$$s = \begin{cases} 11.5 \tilde{f}_p^{-7.5} \tilde{f}^{5.5}, & f \leq f_p \\ 11.5 \tilde{f}^{-2.5}, & f \geq f_p \end{cases} \quad (4)$$

where the dimensionless frequencies are $\tilde{f} = U/C$ and $\tilde{f}_p = U/C_p$ (U =wind speed and C =phase speed). In deep water, these become $\tilde{f} = 2\pi f U/g$ and $\tilde{f}_p = 2\pi f_p U/g$; and the maximum value of s becomes $s_{\max} = 11.5 \tilde{f}_p^{-2.5} = 11.5 (2\pi f_p U/g)^{-2.5}$ at $f = f_p$. Using the dimensionless frequencies in deep water condition, Goda and Suzuki (1975) rewrote the spreading parameter s as

$$s = \begin{cases} s_{\max} \cdot (f/f_p)^5, & f \leq f_p \\ s_{\max} \cdot (f/f_p)^{-2.5}, & f \geq f_p \end{cases} \quad (5)$$

The peak direction, θ_p is the same for all frequencies and the directional spreading function given by Eqs. (2) and (3) is always symmetric about the peak direction, but the degree of spreading varies differently on either side of the peak frequency f_p . The spreading parameter s is high-valued (i.e., the energy is narrowly distributed in direction) at frequencies around the peak frequency and low-valued at frequencies away from the peak.

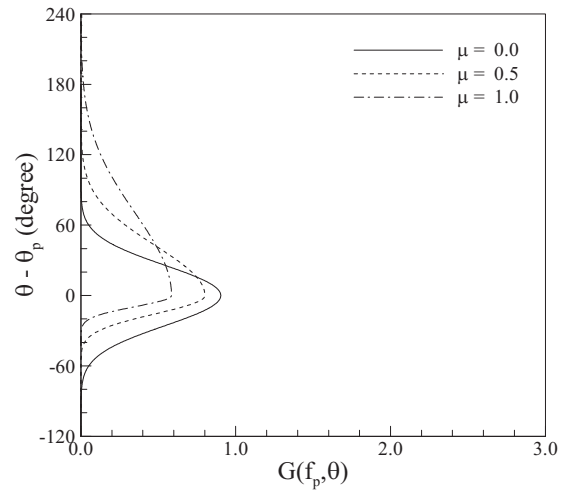
In this study we suggest a directional spreading function that considers directional asymmetry as well as symmetry. The suggested function is given by

$$G(f, \theta) = G_0 \cos^{2s} \left(\frac{\theta - \theta_p}{2} \xi \right) \quad (6)$$

where

$$\xi = \begin{cases} \exp(-\mu), & \theta \geq \theta_p \\ \exp(+\mu), & \theta \leq \theta_p \end{cases} \quad (7)$$

(a)



(b)

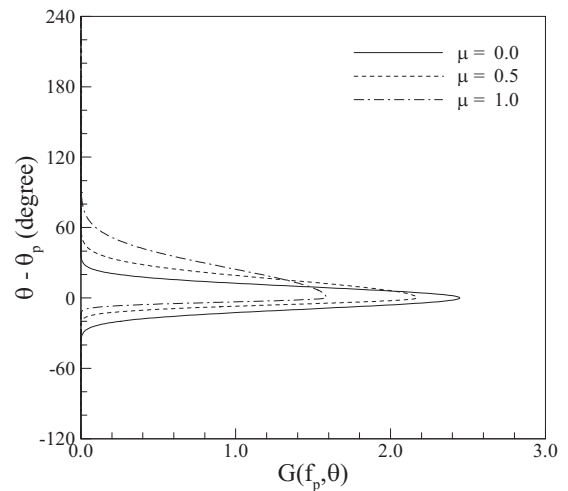


Fig. 1. Variation of directional spreading function $G(f_p, \theta)$ with asymmetry parameter μ at $f = f_p$: (a) $s_{\max} = 10$; (b) $s_{\max} = 75$

$$G_0 = \left[\int_{\theta_{\min}}^{\theta_{\max}} \cos^{2s} \left(\frac{\theta - \theta_p}{2} \xi \right) \right]^{-1} \quad (8)$$

The asymmetry parameter μ is positive when the left-side components (i.e., positive directional components relative to the peak direction, see Fig. 1) from the peak wave direction θ_p are more broadly distributed than the right-side components. When the directional spreading function is symmetric, the asymmetry parameter μ is zero and the present function given by Eqs. (6)–(8) is the same as that of Longuet-Higgins et al. (1961) given by Eqs. (2) and (3). We use only one parameter μ to describe both right- and left-side components of asymmetric distribution, which is quite convenient in expressing real sea spectra. In Eq. (6) we can get the lower and upper limits of wave direction as $-\pi/2 \leq (\theta - \theta_p)\xi/2 \leq \pi/2$. Thus, we have $\theta_{\min} = \theta_p - \pi \exp(-\mu)$ and $\theta_{\max} = \theta_p + \pi \exp(+\mu)$ and the difference between the two limits is given as $\theta_{\max} - \theta_{\min} = \pi[\exp(\mu) + \exp(-\mu)] \geq 2\pi$. However, the difference should be $\theta_{\max} - \theta_{\min} \leq 2\pi$. To overcome this problem, we use the following two conditions:

$$\theta_{\max} - \theta_{\min} = 2\pi \quad (9)$$

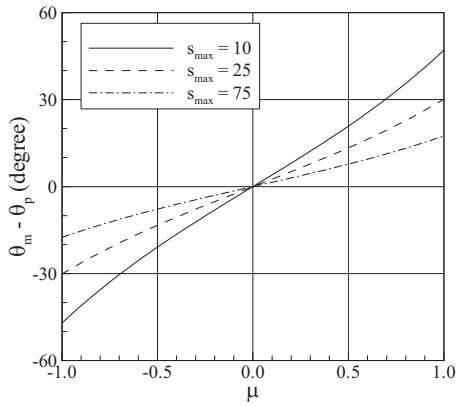


Fig. 2. Variation of mean wave direction θ_m with asymmetry parameter μ at $f=f_p$

$$G(f, \theta_{\min}) = G(f, \theta_{\max}) \quad (10)$$

Thus, we get the directional limits as

$$\theta_{\min} = \theta_p - \frac{2\pi}{1 + \exp(2\mu)}, \quad \theta_{\max} = \theta_p + \frac{2\pi}{1 + \exp(-2\mu)} \quad (11)$$

Fig. 1 shows the directional spreading function at the peak frequency, $G(f_p, \theta)$, for a range of asymmetry parameter values ($\mu=0, 0.5, 1.0$) and spreading parameters ($s_{\max}=10, 75$). For $\mu=0$, the function is symmetric. For $\mu>0$, the left-side components from θ_p are more broadly distributed than the right-side components. For $\mu=1$ and $s_{\max}=10$, the upper and lower limits of wave direction are $\theta_{\max} - \theta_p = 317^\circ$ and $\theta_{\min} - \theta_p = -43^\circ$. However, the spreading function at the limits of wave direction is negligibly small. When the spreading parameter s_{\max} is larger, the spreading function is narrower and more peaked.

The skewness λ_3 is used to measure asymmetry of the directional distribution about the peak direction and is given as (Kreyzig 1999)

$$\lambda_3 = \frac{E[(\theta - \theta_m)^3]}{E[(\theta - \theta_m)^2]^{3/2}} \quad (12)$$

where

$$E[(\theta - \theta_m)^n] = \int_{\theta_{\min}}^{\theta_{\max}} (\theta - \theta_m)^n G(f, \theta) d\theta \quad (13)$$

$$\theta_m = \int_{\theta_{\min}}^{\theta_{\max}} \theta G(f, \theta) d\theta \quad (14)$$

In Eq. (14), the mean wave direction θ_m may be different from the peak wave direction θ_p . If $\lambda_3=0$, the directional distribution is symmetric, and the mean and peak wave directions are equal. If $\lambda_3>0$, the left-side components from the peak wave direction θ_p are more broadly distributed than the right-side components.

Figs. 2 and 3 show variations of the mean wave direction θ_m at the peak frequency ($f=f_p$) and the skewness λ_3 , respectively, with the asymmetry parameter μ . The three cases with $s_{\max}=10, 25, 75$ are shown. As the magnitude of μ increases, so does the magnitude of $\theta_m - \theta_p$. As s_{\max} is larger, the distribution is narrower and thus the magnitude of $\theta_m - \theta_p$ is smaller. Also, as s_{\max} increases, λ_3 is slightly more affected by μ .

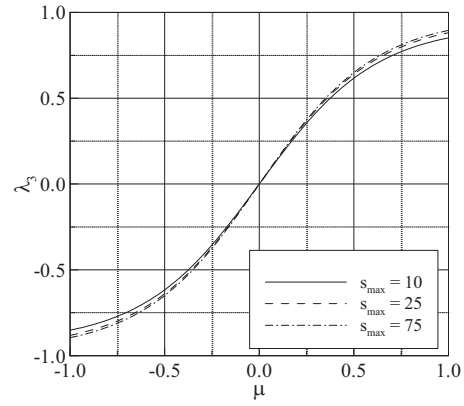


Fig. 3. Variation of skewness λ_3 with asymmetry parameter μ at $f=f_p$

Refraction of Multidirectional Random Waves over a Planar Slope

We conducted numerical experiments to simulate the shoaling and refraction of linear, multidirectional random waves over a planar slope. The exact solution is obtained by first decomposing the energy spectrum into individual frequency and direction bins and applying Snell's law and linear shoaling to each component. Then we find the best-fit of the directional spreading functions to the (exact) calculated spectra.

As an initial condition, we consider a directionally symmetric wave field in a water depth of 166 m ($h/(L_p)_0=1$) with $H_{1/3}=5$ m, $T_{1/3}=10$ sec. We also consider a range of spreading parameters $s_{\max}=10, 75$, and peak directions $\theta_p=0^\circ, 30^\circ$, and 60° , which are the same for all frequencies in the distribution. For the distribution of energy in frequency space we use the JONSWAP spectrum (Hasselmann et al. 1973; Goda 2000), which is expressed as

$$S(f) = \beta_J H_{1/3}^2 T_p^{-4} f^{-5} \exp[-1.25(T_p f)^{-4}] \gamma \exp[-(T_p f - 1)^2/2\sigma^2] \quad (15)$$

$$\beta_J \cong \frac{0.0624}{0.23 + 0.0336\gamma - 0.185(1.9 + \gamma)^{-1}} [1.094 - 0.01915 \ln \gamma] \quad (16)$$

$$T_p \cong T_{1/3} [1 - 0.132(\gamma + 0.2)^{-0.559}] \quad (17)$$

$$\sigma = \begin{cases} \sigma_a = 0.07: & f \leq f_p \\ \sigma_b = 0.09: & f \geq f_p \end{cases} \quad (18)$$

$$\gamma = 1 \sim 7 \text{ (mean value of 3.3 is used here)} \quad (19)$$

Fig. 4 shows the directional spectrum at a water depth of 166 m for $s_{\max}=10$. After decomposing the wave energy into frequency and direction components, the refraction and shoaling of each component is calculated by

$$S_2(f, \theta_2) df d\theta_2 = S_1(f, \theta_1) K_s^2 K_r^2 df d\theta_1 \quad (20)$$

where $K_s = \sqrt{(C_g)_1 / (C_g)_2}$ = shoaling coefficient; $K_r = \sqrt{\cos \theta_1 / \cos \theta_2}$ = refraction coefficient; $C_g = C[1 + 2kh / \sinh(2kh)] / 2$ = group velocity; and $C = \omega / k$ = phase speed. The subscripts 1 and 2 imply the offshore and nearshore spectra, respectively. The wave direction θ_2 is given by Snell's law,

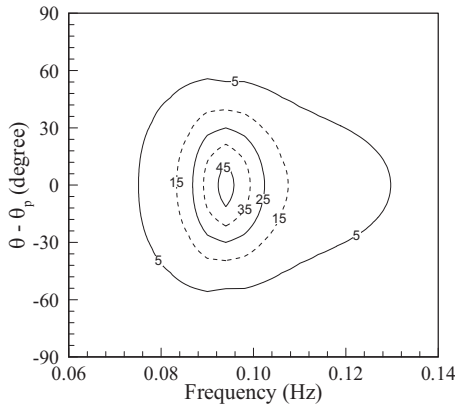


Fig. 4. Input JONSWAP spectrum (unit: m^2/Hz , $H_{1/3}=5$ m, $T_{1/3}=10$ sec, and $s_{max}=10$)

$\sin \theta_2/C_2 = \sin \theta_1/C_1$. At the nearshore location the total wave energy is computed by summing the refracted and shoaled spectrum.

According to Snell's law, the amount of wave refraction between two locations is dependent on wave frequency, even though the dominant wave direction θ_p applies to all frequencies in the offshore region (i.e., the wave generation region), whereas at nearshore locations, θ_p will show a variation with frequency due to the effect of wave refraction. Fortunately, we can make an a priori estimate of the variation of the peak direction with frequency, $\theta_{p2}(f)$, at the nearshore location based only on knowledge of the expected peak direction at the peak frequency, $\theta_{p2}(f_p)$. Since all analytic directional spreading functions require the local peak direction as an input, this method requires no further information than previous methods.

For example, if we assume that the waves at the nearshore location were originally generated with symmetric spreading in deep water, the peak wave angle in deep water is given by

$$\theta_{p0} = \sin^{-1} \left[\frac{C_0(f_p)}{C_1(f_p, h)} \sin \theta_{p2}(f_p) \right] \quad (21)$$

Once the deep water wave direction is known, the peak direction at the nearshore site for each frequency is given by

$$\theta_{p2}(f, h) = \sin^{-1} \left[\frac{C_2(f, h)}{C_0(f)} \sin \theta_{p0} \right] \quad (22)$$

Next, we find the directional spreading function that best fits the nearshore directional spectra. Comparisons are made between the spreading given by the present method using Eqs. (6)–(8) and by the Goda and Suzuki's method using Eqs. (2) and (3). The percent error in the best-fit spectra is denoted E_p and defined as

$$E_p = \frac{\sum_{i=1}^{i_{max}} \sum_{j=1}^{j_{max}} |En_{i,j} - Ee_{i,j}|}{\sum_{i=1}^{i_{max}} \sum_{j=1}^{j_{max}} Ee_{i,j}} \times 100(\%) \quad (23)$$

where Ee =exact wave energy which is calculated by using the Snell's law for each wave energy component; En =wave energy of the best-fit to the exact spectrum; and the subscripts i and j denote the i th frequency and j th directional component, respectively. To get the exact solution, the total wave energy is divided into 51 frequency components and 181 directional components, with $\Delta f=0.004$ Hz and $\Delta \theta=1.0^\circ$, respectively.

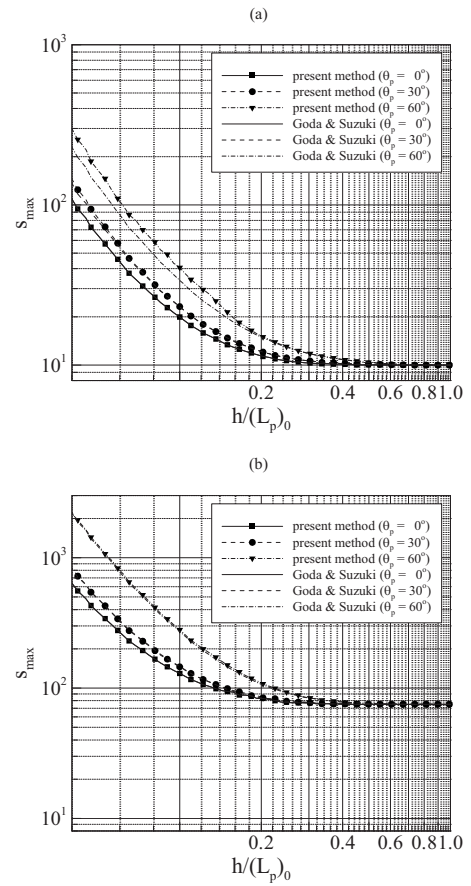


Fig. 5. Variation of spreading parameter s_{max} with relative water depth $h/(L_p)_0$: (a) $s_{max}=10$ in deep water; (b) $s_{max}=75$ in deep water

Fig. 5 shows variation of the spreading parameter s_{max} , as calculated by either the present method or that of Goda and Suzuki, with relative water depth $h/(L_p)_0$ where $(L_p)_0$ =deep-water wavelength. For all the cases, the spreading parameter s_{max} increases as the water depth becomes shallower. For larger deep-water peak wave directions, $(\theta_p)_0$, the spreading parameter, s_{max} , increases faster in shallow water. If the offshore peak wave direction $(\theta_p)_0$ is larger, then waves will experience more refraction, and thus more components of direction will be focused to an angle. For $(\theta_p)_0=0^\circ$, the two methods give the same value of s_{max} . However, for $(\theta_p)_0 \neq 0^\circ$, the present method yields higher value of s_{max} than the Goda and Suzuki method. This implies that, if directional asymmetry is considered, then the wave directions are more narrowly distributed.

Fig. 6 shows variation of the asymmetry parameter μ with relative water depth $h/(L_p)_0$ for the same deep water conditions as in Fig. 4. For $(\theta_p)_0=0^\circ$, the asymmetry parameter μ is zero in all the water depths. However, for $(\theta_p)_0 > 0^\circ$, the asymmetry parameter μ is negative and the magnitude increases as water depth becomes shallower. For narrower deep water directional distributions (i.e., larger s_{max}), there is less refraction of the directional components and the magnitude of μ increases less in shallow water.

Figs. 7–9 show the exact and best-fit directional spectra at the nearshore location ($h=10$ m) for the cases of $(\theta_p)_0=0^\circ, 30^\circ$, and 60° , respectively. The top and bottom portions of each figure compare the exact solution to the best-fit solution from the present method and that of Goda and Suzuki, respectively. Initially the spreading parameter is set to $s_{max}=10$ at $h=166$ m for

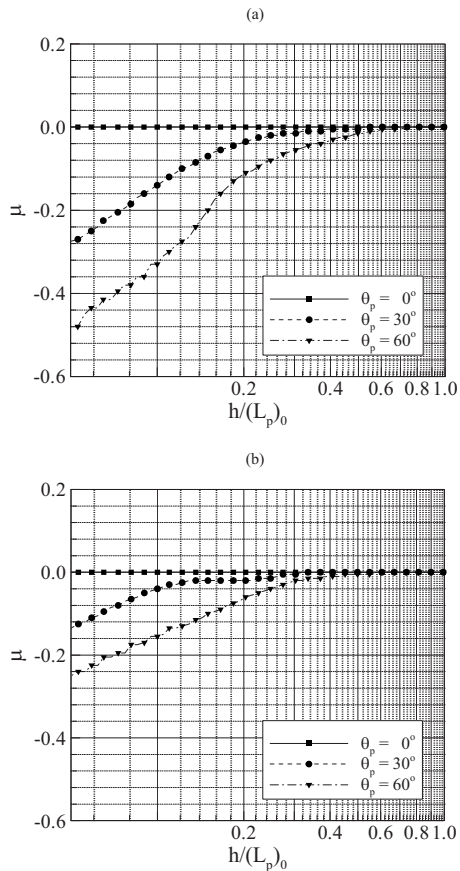


Fig. 6. Variation of asymmetry parameter μ with relative water depth $h/(L_p)_0$: (a) $s_{\max}=10$ in deep water; (b) $s_{\max}=75$ in deep water

all cases, the spectrum of which is shown in Fig. 4. The peak wave angle as a function of frequency, $\theta_p(f, h=10 \text{ m})$, is expressed by a solid line in Figs. 7–9. In Fig. 7(a) there is no variation in θ_p because the deep-water peak direction is shore normal (i.e., $(\theta_p)_0=0^\circ$) for all frequencies. In Figs. 8 and 9 the peak wave direction for $(\theta_p)_0 \neq 0^\circ$ is not shore normal and the peak direction tends toward more shore normal at lower frequencies due to refraction. This phenomenon is more prominent at $(\theta_p)_0=60^\circ$. It is evident from these figures that allowing the peak direction to vary with frequency due to wave refraction better represents the exact directional spectra. Initially some component with $(\theta_p)_0=60^\circ$ travel offshore (i.e., $(\theta)_0 > 90^\circ$) and thus these components do not exist at the nearshore location (see Fig. 9).

For the initial condition $(\theta_p)_0=0^\circ$ (Fig. 7), the directional spreading function becomes more narrowly distributed from $s_{\max}=10$ at $h=166 \text{ m}$ to $s_{\max}=41.4$ at $h=10 \text{ m}$ due to refraction. The two best-fit spreading functions are the same because the initial condition is shore normal and refraction affects both negative and positive directions equally. Hence, the initial symmetric distribution remains so. Figs. 8 and 9 show that asymmetry increases as the initial incident wave angle, θ_p , becomes more oblique. At $h=166 \text{ m}$, the initial parameter values are $s_{\max}=10$, $\mu=0$, and $\lambda_3=0$. At $h=10 \text{ m}$, the parameters become $s_{\max}=51.5$, $\mu=-0.24$, and $\lambda_3=-0.34$ for $(\theta_p)_0=30^\circ$, and $s_{\max}=98.1$, $\mu=-0.44$, and $\lambda_3=-0.56$ for $(\theta_p)_0=60^\circ$. The figures also show that the right-side components from θ_p (i.e., the components on the side closer to $\theta=0^\circ$) are more broadly distributed than the left-side components and thus both values of μ and λ_3 are negative at $h=10 \text{ m}$.

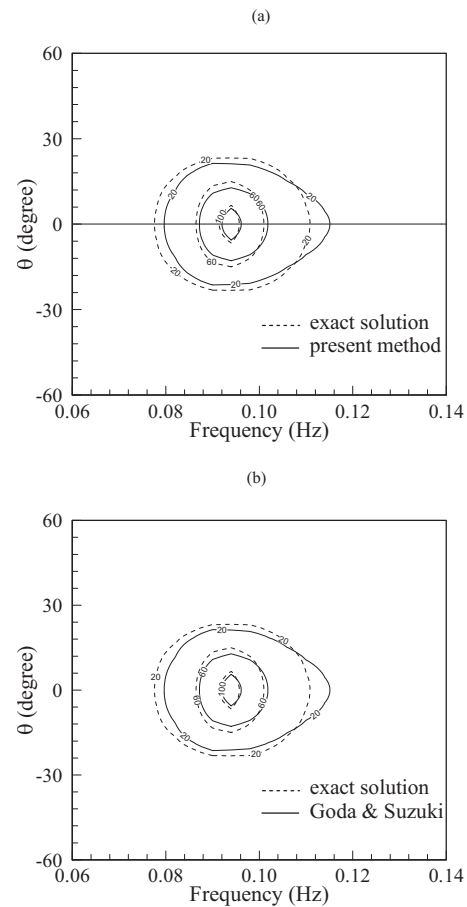


Fig. 7. Comparison of best-fit directional wave spectrum to exact solution at $h=10 \text{ m}$ ($(\theta_p)_0=0^\circ$ and $s_{\max}=10$ in deep water): (a) present method; (b) Goda and Suzuki's method

We can see from Figs. 8 and 9 that, at $h=10 \text{ m}$, the present directional spectrum is closer to the exact solution than the spectrum of Goda and Suzuki. For $(\theta_p)_0=60^\circ$, the percent errors in the spectra of the present method and Goda and Suzuki are $E_p=33$ and 63% , respectively. Fig. 10 compares the percent errors, given by both the present method and Goda and Suzuki's method, relative to the exact solution. The figure also shows the variation of the percent errors, E_p , with relative water depth $h/(L_p)_0$ for $(\theta_p)_0=0^\circ$ and 60° . It is evident that the present method yields less error in all water depths. The percent error for $(\theta_p)_0=0^\circ$ (which is the same for both methods) is also shown in the figure for comparison. The percent error for $(\theta_p)_0 \neq 0^\circ$ is always greater, for either method, than for the case of $(\theta_p)_0=0^\circ$, which indicates the importance of including refractive effects in the analytic spreading function. However, as the water depth becomes shallower the error of the present solution becomes close to the error for $(\theta_p)_0=0^\circ$. This implies that, in very shallow water, all the directional wave components become almost equally focused due to refraction no matter of the deep water wave direction. For the case of $(\theta_p)_0=30^\circ$ and $h/(L_p)_0=0.05$, the Goda and Suzuki's method yields 35% error whereas the present method yields only 25% error. Notably, for the case of $(\theta_p)_0=0^\circ$ and $h/(L_p)_0=0.05$, both methods yielded 25% error.

As shown in Fig. 10, there exist nonzero errors even with the present method which considers directional asymmetry in refracting waves. This is due to the fact that each wave component of frequency and direction experiences differently refraction and

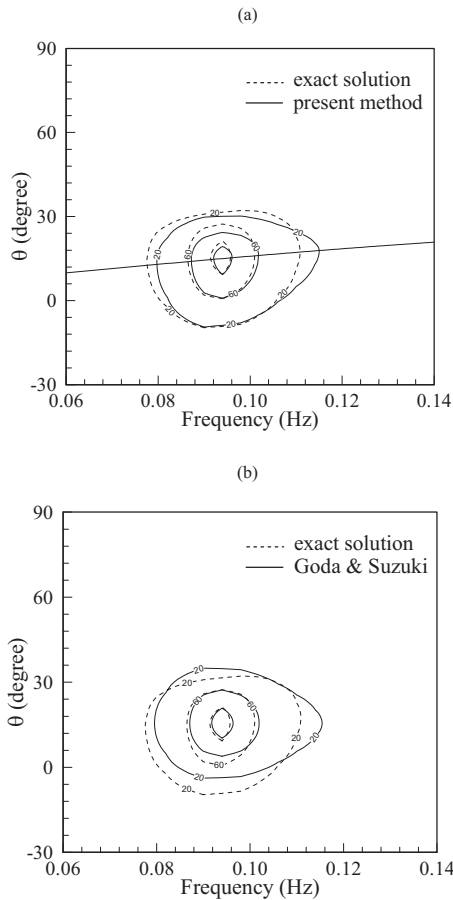


Fig. 8. Comparison of best-fit directional wave spectrum to exact solution at $h=10$ m ($\theta_p=30^\circ$ and $s_{\max}=10$ in deep water): (a) present method; (b) Goda and Suzuki's method

shoaling which cannot be perfectly expressed by one representative value of s_{\max} and μ . Second, fixed values 5 and -2.5 , the exponents of (f/f_p) in the spreading parameter s given by Eq. (5) may change in shallower water. The determination of optimum values of the exponent in each water depth may yield smaller error than the present method. However, optimum values of the exponent depend on many conditions, i.e., the frequency spectrum $S(f)$ with several parameters and the directional spreading function $G(f, \theta)$ with parameters of s_{\max} and $(\theta_p)_0$. In the future, we need to determine optimum values of the exponent in the spreading parameter for several cases of frequency spectrum and directional spreading function.

In the numerical experiments, we showed the cases of broad ($s_{\max}=10$) and narrow ($s_{\max}=75$) directional spreading, but only one case of relatively wide ($\gamma=3.3$ wind-sea condition) frequency spreading. We also tested for the cases of narrower ($\gamma=7$ swell condition) frequency spreading. Even with the increase of peak enhancement factor γ , best-fit values of the spreading parameter s_{\max} and the asymmetry parameter μ do not change noticeably.

In the JONSWAP spectrum given by Eq. (15), the values of $H_{1/3}$, T_p , and γ determine the directional spectrum. However, refraction is prominently affected by both relative water depth and incident wave direction not by $H_{1/3}$ and T_p . It was found through numerical tests that different values of γ do not noticeably affect best-fit values of s_{\max} and μ . Therefore, Figs. 5 and 6 can be used as guidance for the values of the spreading parameter s_{\max} and the asymmetry parameter μ , respectively, given offshore conditions

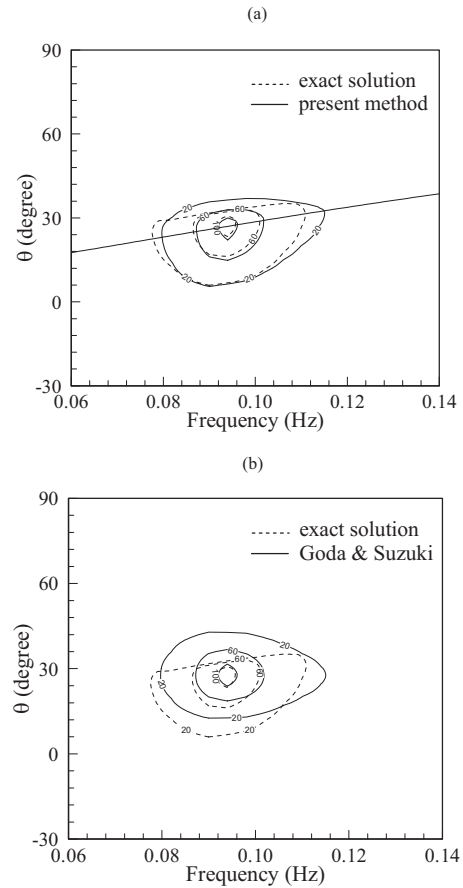


Fig. 9. Comparison of best-fit directional wave spectrum to exact solution at $h=10$ m ($\theta_p=60^\circ$ and $s_{\max}=10$ in deep water): (a) present method; (b) Goda and Suzuki's method

of both the wave direction $\theta_p=0^\circ, 30^\circ, 60^\circ$ and the spreading parameter $s_{\max}=10, 75$.

Comparison of Suggested Directional Spectra to Field Data

Limited evidence of asymmetric directional spreading in water depths of 15 and 5 m can be found in Sanil Kumar et al. (1999) and Sundar et al. (1998), respectively. Herein, as a test of the new asymmetric directional spreading function, we compare the function to directional spectra measured at the U.S. Army Corps of Engineers Field Research Facility at Duck, NC. Measured spectra were calculated using data from a long duration, bidirectional array of 15 bottom-mounted pressure sensors deployed in a water depth of 8 m [the "eight-meter array," see Long and Oltman-Shay (1991)]. These data are unique in that the measurements of the wave directional distributions are much more highly resolved than those obtained by wave buoys or smaller arrays. Approximately six months of archived spectra, collected every three hours from January through June 2006 for a total of 1,383 spectral records, were used for the comparison.

The range of wave conditions contained in these data are shown in Fig. 11. The wave conditions consist of some long period swell as well as higher-frequency wind seas with a wide range of incident wave angles. The data also include some very high angle high-frequency conditions. Wave angles represent directions of wave approach between -90° and 90° and increasing

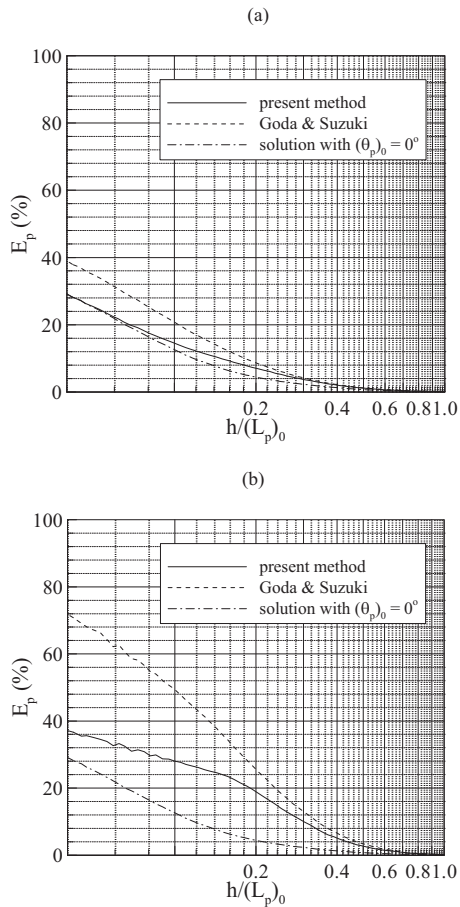


Fig. 10. Variation of percent error in wave energy with relative water depth $h/(L_p)_0$: (a) $(\theta_p)_0=30^\circ$; (b) $(\theta_p)_0=60^\circ$

counterclockwise from shore normal (0°). After windowing and frequency band-averaging, all archived spectra had a resolution of 0.0098 Hz and 2° , and the resolved frequency range was $0.04 < f < 0.32$ Hz with 160 degrees of freedom.

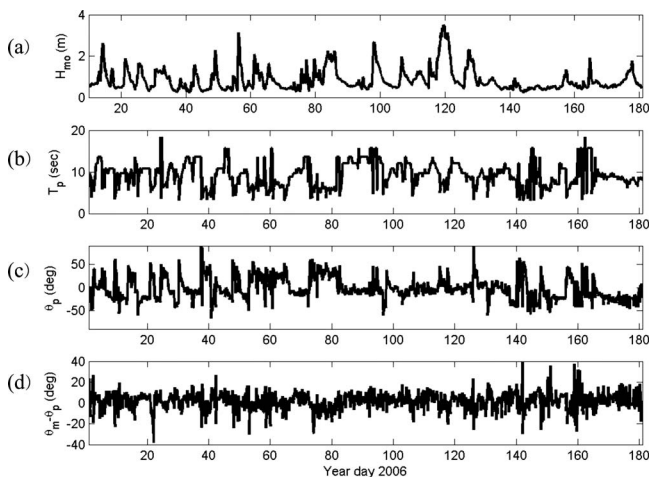


Fig. 11. Six months of wave conditions measured at the FRF 8-m array: (a) H_{m0} ; (b) T_p , peak period; (c) θ_p , peak direction (i.e., peak direction at the peak period); and (d) difference between the mean direction and peak direction at the peak period

Table 1. Correlation Coefficients between the Best-Fit Asymmetry Parameter μ , the Measured Peak Direction θ_p , the Measured Mean Direction θ_m , and $\theta_m - \theta_p$

	θ_p	θ_m	$\theta_m - \theta_p$
μ	-0.61	-0.40	0.82
θ_p		0.95	-0.69
θ_m			-0.43

Differences between the mean direction and the peak direction, $\theta_m - \theta_p$, are indicative of the skewness of the directional distribution. The time series shown in Fig. 11(d) suggests that skewed distributions and hence, directional asymmetries are common at this coastal site and that the asymmetry is caused by wave refraction. The influence of refraction is evident by the fact that the median value of $\theta_m - \theta_p$ for $\theta_p > 0$ is -5.2° and $+5.1^\circ$ for $\theta_p < 0$. Since refraction will skew the distributions toward shore normal, refraction-induced skewness causes $\theta_m - \theta_p$ to be oppositely signed from θ_p . As further confirmation, Table 1 shows that θ_p and $\theta_m - \theta_p$ are negatively correlated.

The effects of refraction on the measured directional spectra are also evident by visual examination. For example, the measured directional spectra shown in Figs. 12(a and c) show a trend in the peak direction that depends on frequency. Using Eq. (22) and the measured peak direction at the peak frequency, the expected refraction-induced variations in peak direction as a function of frequency were calculated and shown as black lines in the figure. These estimated wave directions well match the observed trend in the measured peak wave angles, which demonstrates the fingerprint that refraction leaves on the nearshore spectrum.

Next, we examine whether the asymmetric spreading function and accounting for refraction-induced changes in wave angle better represents the measured spectra when compared to the traditional symmetric spreading function. For each measured directional spectrum, the best-fit asymmetry (μ) and spreading

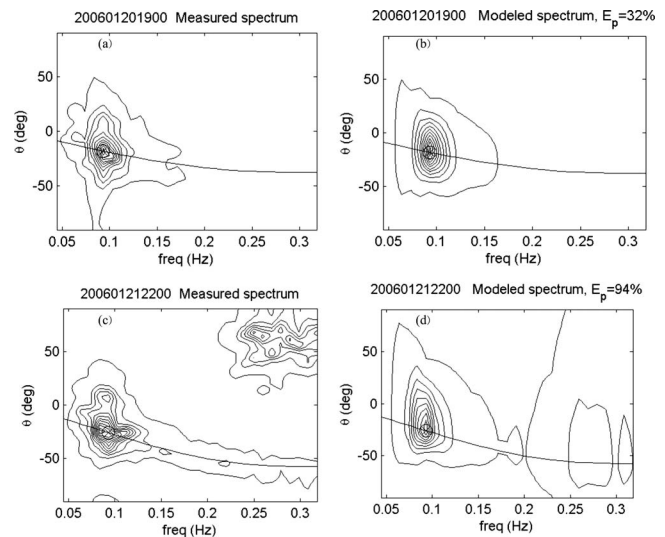


Fig. 12. Measured directional spectra for (a) January 20, 19:00 EST, $f_p=0.093$ Hz, $\theta_p=-18^\circ$; (c) January 21, 22:00 EST, $f_p=0.093$ Hz, $\theta_p=-26^\circ$; corresponding model spectra (b) $s_{max}=27.5$, $\mu=0.15$; and (d) $s_{max}=25$, $\mu=0.45$. Black lines represent $\theta_{p2}(f)$ based on assuming a uniform peak direction in deep water for all frequencies

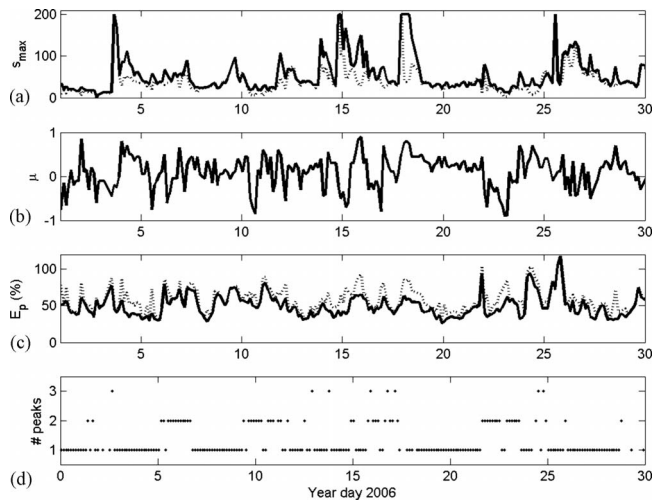


Fig. 13. (a) Time series of best-fit s_{\max} ; (b) best-fit μ ; (c) percent error; dashed line=symmetric function, solid line=asymmetric function; and (d) number of measured spectral peaks

parameters (s_{\max}) were found through a two-dimensional search. Resolution of the parameter search was $\Delta s_{\max}=2.5$ and $\Delta\mu=0.05$, with a range of $0 < s_{\max} < 200$ and $-1 < \mu < 1$. The function-data percent errors were calculated using Eq. (23), where the “exact” solution is now the measured directional distribution over all resolved frequencies and wave directions. The best-fit parameters were those corresponding to the minimum error. In a similar fashion, the best fit s_{\max} and the minimum errors were also found for the symmetric distribution ($\mu=0$) including the correction to the peak directions from Eq. (22). Finally, it should also be noted that the functional spectra were scaled such that the total energy in the region $\theta_{\min} < \theta < \theta_{\max}$ is equal to the measured $S(f, -90^\circ < \theta < 90^\circ)$.

Time series of the best-fit s_{\max} and μ values along with the calculated function-data errors are shown in Fig. 13 for both the symmetric and asymmetric functions. The time series is limited to 30 days for plotting clarity. The figure clearly shows that the functional error is reduced when considering asymmetry. The mean errors for the asymmetric and symmetric functions, averaged over the six-month data set, were 50% and 58%, respectively. For completeness, the mean error for using the symmetric function without the peak direction correction was also calculated, and it only made a minor difference for the symmetric function (59%). Fig. 13(a) shows that the asymmetric function tends to increase the optimal s_{\max} parameter, which means waves are more narrowly focused to the peak direction.

Figs. 12(b and d) show examples of best-fit directional spectra corresponding to the measured spectra in Figs. 12(a and c), respectively. These spectra also highlight one source of error in the comparison between the measured and best-fit spectra. The spectrum in Fig. 12(b) is a good fit with relatively low error (32%). However, in Fig. 12(d) the error has risen to 94%. It is apparent that the increase in error is being driven by the fact that a secondary spectral peak has appeared in the measurements. As can be seen in Fig. 12(d), wind-seas are bimodal at frequencies greater than the peak frequency (Ewans 1998; Hwang et al. 2000). The secondary spectral peak near 0.28 Hz and 60° is the result of a passing weather front at the nearshore field site (which increased the wind speed and rotated the wind direction) and the

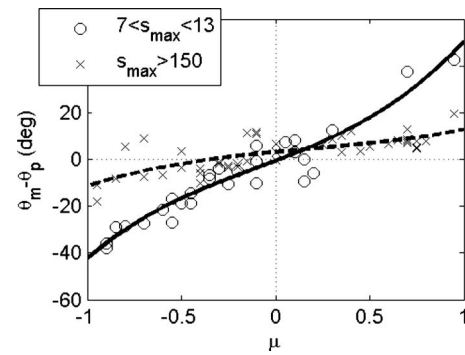


Fig. 14. Measured $\theta_m - \theta_p$ versus best-fit asymmetry parameter; μ ; solid line=fourth-order polynomial fits to $7 < s_{\max} < 13$, dashed line=fourth-order polynomial fits to $s_{\max} > 150$

generation of a developing wind sea. It can be seen at high frequencies in Fig. 12(d) that the fitting procedure is attempting to spread the high-frequency energy across the directional range to capture the wind wave energy arriving from positive angles. However, we would note that it has already been known that empirical directional spectral models, such as are used herein, are not designed to simulate multi-peaked spectra. For simplicity, we have not manually removed these secondary spectral peaks, which are not relevant to the analysis, from the measured spectra. In Fig. 13(d) a time series of the number of separable peaks in the frequency spectra are also plotted. Time of bimodal and trimodal spectra generally appears to coincide with increased errors in both directional distribution functions. Removing the secondary peaks in the calculation of the best-fit spectra would clearly reduce the error further. Nonetheless, despite the relatively large overall error in Fig. 12(d), the peak around 0.09 Hz is well captured by the best-fit spectrum.

The presence of a highly oblique high-frequency wind sea highlights another aspect of the present model. Even in the case of a single peak frequency, it is possible that the peak wave direction at the nearshore site is sufficiently oblique that it cannot be the result of the refraction of waves generated in deep water. In such cases, Eq. (22) predicts that the deep water wave angles would be greater than 90° , which is not physically possible. For these cases it is better to simply leave the peak direction independent of frequency as in previous methods. However, here we have not included spectra with these conditions in our analysis.

Finally, as shown in Refraction of Multidirectional Random Waves over a Planar Slope through the refraction and shoaling of idealized spectra, μ is expected to be correlated with $\theta_m - \theta_p$ and also show a variation with s_{\max} (see Fig. 2). Fig. 14 demonstrates that the best-fit μ values from the present directional spreading function show the appropriate variation with s_{\max} and the measured $\theta_m - \theta_p$. For this figure the best-fit parameters for the asymmetric function were separated into two groups based on their s_{\max} values similar to what was done in Fig. 2. The figure shows that the measured $\theta_m - \theta_p$ values are odd functions (about $\mu=0$) of the best-fit μ values, as expected. Also, as the spreading parameter (best-fit s_{\max}) increases, the slope decreases. In general, the $\theta_m - \theta_p$ versus the best-fit μ from data grouped by spreading parameter correspond well to the results from idealized spectra shown in Fig. 2. Also, the correlation coefficients listed in Table 1 show that μ is positively correlated with $\theta_m - \theta_p$ and μ has a

negative correlation with θ_p . Both of which are expected results due to refraction-induced asymmetry.

Conclusion

In the present study we developed a more general directional spreading function for multidirectional random waves, which allows for directional distributions of arbitrary asymmetry. Directional asymmetry can be found in real seas where waves are shadowed by islands or man-made structures or in coastal areas where wave refraction is important. This new directional spreading function will allow for more realistic design wave conditions to be used in the modeling of coastal structures both numerically and in laboratory experiments.

For multidirectional random waves over a planar slope, directional spreading functions that best-fit the exact solution were found. For the directional spreading functions two methods were used, i.e., the present method that allows directional asymmetry as well as refraction induced changes to the peak wave directions, and the method of Goda and Suzuki (1975), which considers directional symmetry only. For consistency here, we applied the changes in the peak wave direction to the Goda and Suzuki method as well in our comparisons. The methods were tested numerically using the JONSWAP spectrum as the initial frequency spectrum in deep water. The exact solution of the expected shoaled and refracted directional spectra were obtained by decomposing the wave energy into frequency and direction components, and then applying Snell's law for each wave component. When waves approached the coastline with an oblique peak wave direction, the directional distribution became asymmetric due to wave refraction. For more oblique incident wave directions and in shallower relative water depths, refraction induced asymmetry became more significant. The present method expressed the refraction and shoaling of wave energy more accurately than the Goda and Suzuki method. As a test of the new asymmetric directional spreading function, we compared the function to directional spectra measured at the U.S. Army Corps of Engineers Field Research Facility at Duck, NC. The measured data showed that directional asymmetry is common at this coastal site and the asymmetry is caused by wave refraction. Also, time series of the best-fit s_{\max} and μ values along with the calculated function-data errors show that the functional error is reduced when asymmetry and refractive effects on the peak wave direction are considered.

Acknowledgments

This work was supported by the Korea Science and Engineering Foundation (KOSEF) grant funded by the Korea government (MEST) (Grant No. R01-2008-000-20442-0). We thank the staff at the FRF for making their extensive observations available online and all of their efforts at ongoing data collection. We also thank Patricio Catalán for providing code to read the measured spectra.

References

- Borgman, L. E. (1969). "Directional spectral models for design use." *Proc., Offshore Technology Conf.*, Houston, Paper No. OTC1069, 721–746.
- Bouws, E., Günther, H., Rosenthal, W., and Vincent, C. L. (1985). "Similarity of the wind wave spectrum in finite depth water." *J. Geophys. Res.*, 90(C1), 975–986.
- Bretschneider, C.L. (1968). "Significant waves and wave spectrum." *Ocean Industry*, 40–46.
- Ewans, K. C. (1998). "Observations of the directional spectrum of fetch-limited waves." *J. Phys. Oceanogr.*, 28(3), 495–512.
- Goda, Y. (2000). *Random seas and design of maritime structures*, World Scientific, River Edge, N.J.
- Goda, Y., and Suzuki, Y. (1975). "Computation of refraction and diffraction of sea waves with Mitsuyasu's directional spectrum." *Rep. No. 230*, The Port and Harbour Research Institute, Japan (in Japanese).
- Hasselmann, K., et al. (1973). "Measurements of wind-wave growth and swell decay during the joint north sea wave project (JONSWAP)." *Deutsches Hydrographisches Zeitschrift*, 8(12), 1–95.
- Hwang, P. A., Wang, D. W., Walsh, E. J., Krabill, W. B., and Swift, R. N. (2000). "Airborne measurements of the wavenumber spectra of ocean surface waves. Part 2: Directional distribution." *J. Phys. Oceanogr.*, 30(11), 2768–2787.
- Kreyszig, E. (1999). *Advanced engineering mathematics*, Wiley, New York.
- Long, C. E., and Oltman-Shay, J. M. (1991). "Directional characteristics of waves in shallow water." *Technical Rep. No. CERC-91-1*, U.S. Army Engineer Waterways Experiment Station, Vicksburg, Miss.
- Longuet-Higgins, M. S., Cartwright, D. E., and Smith, N. D. (1961). "Observations of the directional spectrum of sea waves using the motions of a floating buoy." *Ocean wave spectra*, Prentice-Hall, Englewood Cliffs, N.J., 111–32.
- Mitsuyasu, H. (1970). "On the growth of spectrum of wind-generated waves (2)—Spectral shape of wind waves at finite fetch." *Proc., 17th Japanese Conf. Coastal Engineering*, JSCE, 1–7 (in Japanese).
- Mitsuyasu, H., Tasai, F., Mizuno, S., Ohkusu, M., Honda, T., and Rikishi, K. (1975). "Observation of the directional spectrum of ocean waves using a cloverleaf buoy." *J. Phys. Oceanogr.*, 5(4), 750–760.
- Pierson, W. J., and Moskowitz, L. (1964). "A proposed spectral form for fully developed wind seas based on the similarity theory of S.A. Kitaigorodskii." *J. Geophys. Res.*, 69(24), 5181–5190.
- Pierson, W. J., Tuttle, J. J., and Wooley, J. A. (1952). "The theory of the refraction of a short-crested Gaussian sea surface with application to the northern New Jersey coast." *Proc., 3rd Conf. Coastal Engineering*, ASCE, Cambridge, Mass., 86–108.
- Sanil Kumar, V., Deo, M. C., Anand, N. M., and Chandramohan, P. (1999). "Estimation of wave directional spreading in shallow water." *Ocean Engineering*, 26(1), 83–98.
- Suh, K. D., Kweon, H.-M., and Yoon, H. D. (2002). "Reliability design of breakwater armor blocks considering wave direction in computation of wave transformation." *Coastal Engineering J.*, 44(4), 321–341.
- Sundar, V., Sannasiraj, S. A., and Kaldenhoff, H. (1998). "Directional spreading of waves in the nearshore zone." *Ocean Engineering*, 26(2), 161–188.
- Van Dongeren, A., Reniers, A., and Battjes, J. (2003). "Numerical modeling of infragravity wave response during DELILAH." *J. Geophys. Res.*, 108(C9), 3288.
- Vuğts, J. H. (2005). "Fatigue damage assessments and the influence of wave directionality." *Appl. Ocean Res.*, 27(3), 173–185.